

Nanomechanical mapping with resonance tracking scanned probe microscope

A B Kos and D C Hurley

National Institute of Standards and Technology, 325 Broadway, Boulder, CO 80305-3328, USA

E-mail: kos@boulder.nist.gov

Received 31 July 2007, in final form 5 October 2007

Published 23 November 2007

Online at stacks.iop.org/MST/19/015504

Abstract

We present a new digital-signal-processor-based resonance tracking system for scanned probe microscopy (SPM) imaging. The system was developed to enable quantitative imaging of mechanical properties with nanoscale spatial resolution at practical data acquisition rates. It consists of a 32-bit floating-point digital signal processor connected to a high-resolution audio coder/decoder subsystem, an rms-to-dc converter and a voltage-controlled oscillator. These components are used in conjunction with a commercial atomic force microscope to create a versatile platform for SPM mechanical mapping. Images of a glass-fibre/polymer matrix composite sample are presented to demonstrate system performance.

Keywords: atomic force acoustic microscopy, atomic force microscope, contact-resonance spectroscopy, digital signal processor, elastic modulus, rms-to-dc converter, scanned probe microscopy

(Some figures in this article are in colour only in the electronic version)

1. Introduction

The trend towards nanometre dimensions in many emerging applications demands new approaches to materials characterization. For example, information about mechanical properties such as elastic modulus, adhesion and friction is often needed. This need is partly motivated by the increasingly common practice of integrating multiple materials, often with very different properties, into a single device or structure. Values of a sample's 'average' properties are therefore no longer adequate. Instead, quantitative images or maps to visualize the spatial distribution in properties are demanded—often with nanoscale lateral resolution.

One instrument that can provide both the spatial resolution and imaging capability required for this challenge is the atomic force microscope (AFM). Accordingly, a variety of scanned probe microscopy (SPM) methods for evaluating mechanical properties have been explored. SPM methods that promise quantitative information typically use dynamic approaches, in which the AFM cantilever is vibrated at or near the frequency of a resonant mode. Atomic force acoustic microscopy (AFAM) [1] is one such technique. In AFAM, the resonant frequencies of the AFM cantilever are measured when the

cantilever tip is in contact with a sample. From the values of these 'contact-resonance frequencies', the sample's elastic properties can be determined [1, 2]. In particular, the contact-resonance frequencies of the cantilever's flexural (bending) modes yield values for the indentation modulus M . For an isotropic material $M = E/(1 - \nu^2)$, where E is Young's modulus and ν is Poisson's ratio. The small radius of the AFM tip (≈ 10 – 100 nm) enables nanoscale spatial resolution.

Although quantitative AFAM methods have been demonstrated for modulus measurements at a stationary position, quantitative modulus *imaging* with contact-resonance spectroscopy methods has not reached its full potential. One reason for this deficiency is that fixed-position techniques involving lock-in or network analyser approaches are typically orders of magnitude too slow for practical imaging [3]. To achieve rapid modulus mapping using contact-resonance methods, we have developed digital-signal-processor (DSP) software and electronics to track the contact-resonance frequencies during imaging [4]. Here we describe the design and operation of this resonance tracking system. The system is designed to operate in conjunction with a commercial AFM, and this symbiosis will be discussed as well. The system is easy to use but still

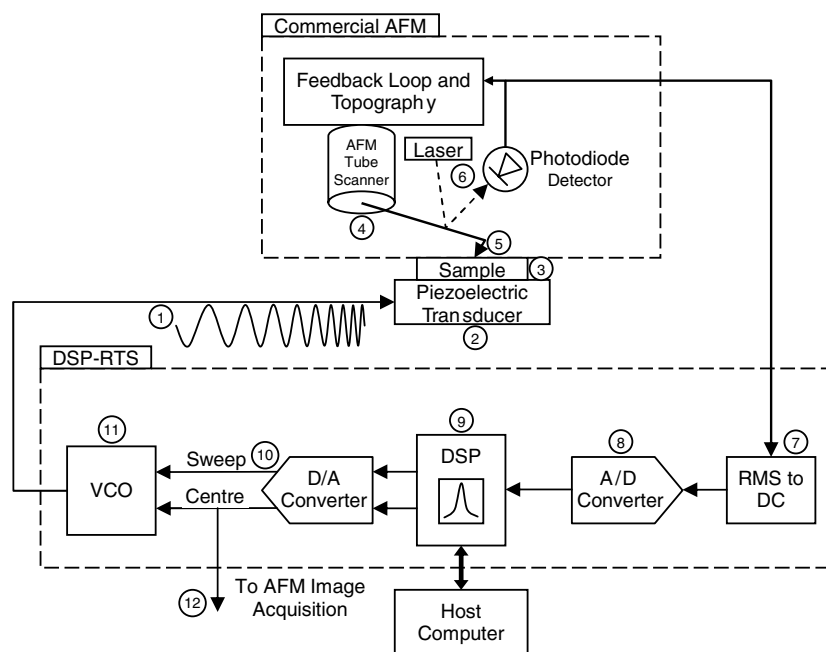


Figure 1. Block diagram of the DSP-based resonance tracking system showing sinusoidal sweep voltage (1), piezo transducer (2), sample (3), AFM tube scanner (4), nanometre-sized tip (5), laser beam-bounce circuit (6), rms-to-dc converter (7), A/D converter (8), DSP (9), D/A converter feedback loop (10), voltage-controlled oscillator (11) and image input to AFM electronics (12).

allows the operator to fine-tune the control parameters for specific experimental conditions (e.g., measurement speed and frequency range). We present images of a glass-fibre/polymer matrix composite sample to illustrate system performance. Our system is intended to perform tasks similar to those achieved in previous work [1, 3, 5, 6], but with reduced imaging times and greater flexibility afforded by the DSP-based approach. We have previously published results [4, 7, 8] using the techniques described in this paper but have not yet published a comprehensive description of the system itself.

2. System description

For quantitative imaging with AFAM or related methods, we need to rapidly detect the peak in the contact-resonance spectrum as the tip is scanned across the sample in contact. Depending on the properties of the sample, the peak frequency could differ substantially in various image locations. Thus, the purpose of our system is to ‘track’ a resonant frequency of the vibrating cantilever. For this reason, we call it a ‘DSP-based resonance tracking system (DSP-RTS)’. The DSP-RTS is modular, and can be understood in terms of its components.

As the measurement platform, we use a Veeco/Digital Instruments Dimension 3000 AFM¹. The most important components of the AFM for this work include a piezoelectric tube scanner for x - y - z motion, a sample x - y positioning stage, the cantilever/tip sensor, a laser/photodiode detection

scheme and control electronics and software. The sensitivity of the photodiode detector in our AFM rolls off at frequencies higher than approximately 2 MHz, although signals up to at least 3 MHz can be detected. For contact-resonance-frequency imaging, we required access to the unfiltered photodiode signal as input for the DSP-RTS. The frequency-proportional output of the DSP-RTS was used as an external input to an auxiliary image channel of the AFM. For signal input/output to the AFM, we used the Signal Access Module accessory. In addition to these AFM components, our contact-resonance experiments required a piezoelectric actuator (Panametrics model V106-RM). The transducer is attached to the bottom of the sample and is used to excite the resonant frequencies of the cantilever over the range 100 kHz to 3 MHz.

Figure 1 shows the block diagram of the apparatus. The basic operation is as follows: an adjustable-amplitude, swept-frequency sine wave (1) is applied to the piezoelectric transducer (2) onto which the sample of interest (3) is mounted. One end of the cantilever (4) is attached to the AFM tube scanner. The opposite end of the cantilever has a nanoscale tip (5) that is maintained in contact with the sample by the AFM feedback control. The motion of the cantilever is monitored by the standard AFM laser beam-bounce approach using a position-sensitive photodiode detector (6). As the cantilever is swept through its resonant frequency by the piezoelectric transducer, the photodiode detects the cantilever’s vibration amplitude and sends this signal to the DSP tracking system. Inside the DSP system, the vibration signal is converted to a voltage proportional to the rms amplitude of vibration (7) and sent to an analogue to digital converter (8). The DSP (9) reads this signal, constructs a complete resonance curve as each sweep completes, finds the peak in the resonance curve, and uses this information in a feedback-control loop (10), adjusting

¹ Commercial equipment and materials are identified in order to adequately specify certain procedures. In no case does such identification imply recommendation or endorsement by the National Institute of Standards and Technology, nor does it imply that the materials or equipment identified are necessarily the best available for the purpose.

a voltage-controlled oscillator (11) to tune the centre frequency of vibration to maintain the cantilever response curve centred on resonance. The control voltage, used to adjust the centre frequency of the voltage-controlled oscillator, is also sent to an auxiliary image input port (12) used by the AFM to plot an image proportional to the resonance frequency.

The system is built around a Texas Instruments (TI) TMS320C6711 DSP Starter Kit (DSK) that incorporates a 150 MHz C6711 32-bit floating-point digital signal processor. Important features of the C6711 are the enhanced direct memory access controller (or memory controller) that allows complete data acquisition without central processor unit (CPU) intervention, the multi-channel buffered serial port (McBSP) that is used to communicate with the analogue to digital (A/D) and digital to analogue (D/A) converters, and the multi-unit processor core, which allows 900 million floating point operations per second to be executed. The A/D and D/A converter used is a TI PCM3003 20-bit delta-sigma stereo audio coder/decoder (codec) daughter-card operating at 48 kilosamples per second (kS s^{-1}). A total of 128 data points are acquired for each resonance curve, and at 48 kS s^{-1} the system is capable of acquiring the full cantilever resonance curve 375 times per second.

The piezoelectric transducer drive voltage is obtained from a wide frequency range, voltage-controlled oscillator (VCO). The VCO has two inputs: a slower responding full range control input and a faster responding sweep input. The sweep input is driven by a triangular sweep voltage from one stereo output of the D/A converter. The slow input is driven by the other D/A converter stereo output using proportional-integral-derivative (PID) feedback control to set the centre frequency. These inputs are both dc coupled. The currently implemented circuit realizes approximately 17–18 bits of resolution, corresponding to a frequency resolution of about 12 Hz over the full-range span of 3 kHz to 3 MHz. This can be improved with the averaging effect of the integral term in the PID control at the expense of a slower response. The output of the oscillator is applied to a user-adjustable amplifier in order to drive the piezoelectric actuator.

Delta-sigma A/D and D/A converters such as those used in the PCM3003 have an intrinsic pipeline delay that is a natural result of the delta-sigma conversion process. This delay occurs between the time the McBSP sends a new sample point to the D/A converter and the time the output voltage from the D/A converter changes to the new value. The delay can be as much as 22 sample periods. (The same is true for the A/D converter, but in the opposite direction.) At 48 kS s^{-1} this corresponds to a 0.92 ms ($22 \times 2 \times 21 \mu\text{s}$) total delay. To compensate for this delay, we added an appropriate advance of 44 sample points to the digital triangular sweep curve to synchronize the sweep curve generation with the data-acquisition process.

A wideband rms-to-dc converter chip fed by a low-noise, high-gain operational amplifier is used to detect the magnitude of the photodiode signal and deliver it to the A/D converter. The rms-to-dc converter has a flat bandpass response from about 1 kHz to 3.2 MHz. Its outputs are ac-coupled to the A/D converter in order to eliminate dc drift errors; this is acceptable

given that the voltage-controlled oscillator sweeps 375 times per second and the audio daughter-card accepts signals in the 10 Hz to 20 kHz range.

The software for the DSP-based resonance tracking system has two components: the real-time control software that runs on the DSK and a user interface that runs on the host computer. The real-time control software is responsible for the following: generating the triangular sweep voltage to the VCO, acquiring the data points necessary to construct the cantilever resonance curve, finding the peak in the resonance curve, computing the required feedback for maintaining the cantilever on resonance based upon the user-defined P, I and D terms, calculating several user parameters and coordinating communication/control with the user host program. The host program is used to enter parameters such as the PID constants, engage the servomechanism and monitor the quality of resonance tracking. User commands and output parameter updates are serviced only when the DSP is idle. The host computer is not critical to this application, and once the operational parameters are entered and the system is operating, the host computer could be disconnected without affecting the image acquisition.

To relieve the CPU of the burden of data acquisition, the memory controller coordinates all aspects of data acquisition and memory transfer. The memory controller alternately outputs the upward-sweeping values of the VCO sweep voltage followed immediately by the downward-sweeping values, in an endless loop. As each sweep point is output, the memory controller also reads the resonance curve data points. At the end of each sweep, the CPU is notified via CPU interrupt that the current resonance curve is ready for processing. This procedure proceeds continuously in a ping-pong fashion, with the memory controller filling one section of memory while the CPU processes the other.

The main task of the CPU is to process the resonance curve data and provide a feedback correction signal to adjust the centre frequency of the VCO. There are many techniques that can be used to calculate the centre frequency of a measured resonance curve contaminated with noise, e.g., fitting the curve to a Lorentzian curve or performing an interpolation and using the fit to determine the feedback. In the current implementation, the CPU simply finds the highest point in the data set and returns its index. With the feedback loop operating at 375 Hz, this simple approach works reasonably well for signals of sufficient strength.

Since the CPU is constantly adjusting the centre frequency of the VCO to keep it on resonance, and the centre frequency voltage is used to produce the AFM image, it would be advantageous if this voltage were perfectly proportional to frequency with a convenient conversion factor (e.g., 1 V corresponds to 1 MHz). This requirement necessitated a change to the DSP-RTS, which will be discussed in more detail later.

2.1. TMS3206711 DSK and PCM3003 codec

The important components of the C6711 DSK and PCM3003 daughter-card are shown in figure 2. The primary elements

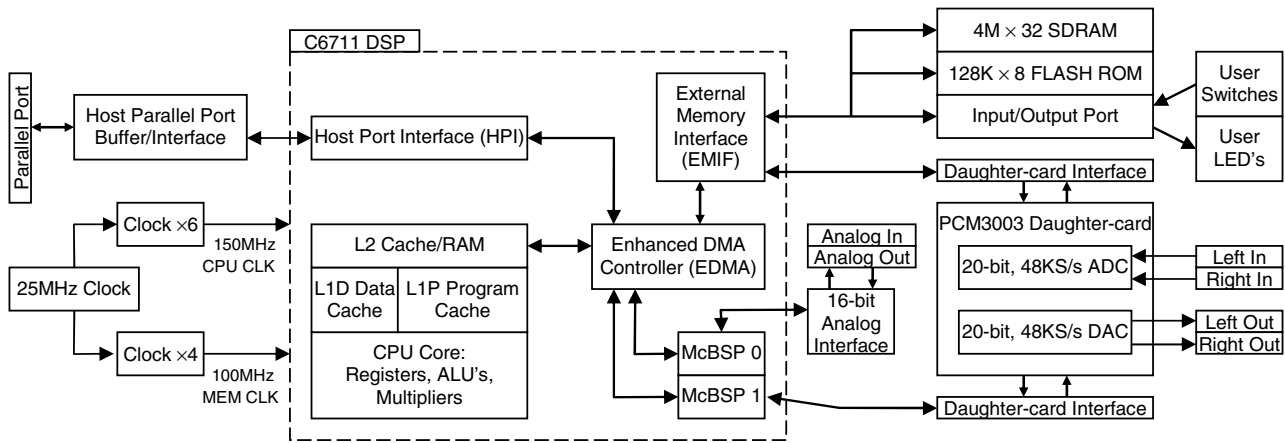


Figure 2. Simplified block diagram of Texas Instruments C6711 DSK with PCM3003 codec daughter-card.

of the C6711 DSK used by the DSP-RTS are: the host-port interface, memory controller, McBSPs, daughter-card interface, 150 MHz DSP core with internal cache and 16-megabyte external RAM and onboard 16-bit analogue interface. The PCM3003 stereo audio codec includes two 48 kS s^{-1} , 20-bit channels of input and output. All four of these channels are used by the DSP-RTS.

The C6711 communicates with the host computer over the host-port interface, which connects to the host computer via its parallel printer interface. This interface allows the host computer to access the entire memory map of the DSP, permitting communication between the host and DSP. Inside the C6711 DSP, the memory controller facilitates bi-directional communication with two serial ports: McBSP0, which connects to the onboard 16-bit codec, and McBSP1, which connects to the PCM3003 stereo codec. The memory controller can maintain a continuous stream of data to these ports, using a ping-pong mechanism to automatically switch back and forth between two memory arrays without intervention from the CPU. The memory controller acquires data from the codec, filling one section of memory while the CPU processes the data in the other section of memory. (For output, it streams one memory section to the codec.) The memory controller generates an interrupt to the CPU when acquisition in one memory section is complete, minimizing CPU overhead costs.

The DSP CPU is equipped with eight independent functional units: four floating-point arithmetic logic units, two fixed-point arithmetic logic units and two floating-point multipliers. Because the units are independent, it is possible to get all or most of the units running in parallel, with appropriate coding. The 900 million floating-point operations per second performance figure is obtained from the fact that there are six floating-point units executing instructions each CPU clock cycle, at a clock frequency of 150 MHz. The C6711 CPU also includes, on-chip, a two-level (L1/L2) cache memory architecture for code and data: a 32 kilobit (4 kilobyte) L1P program cache, a 32 kilobit (4 kilobyte) L1D data cache and a 512 kilobit (64 kilobyte) L2 cache/RAM. The L2 cache/RAM is sufficient to hold the entire current version of the DSP program without the need to access the DSK's

external memory, which improves performance. Thirty-two 32-bit general-purpose registers are provided for address/data manipulation; this is appropriate since memory addresses and most floating-point operands are 32 bits wide. We use floating-point arithmetic almost exclusively in the implementation of the DSP code.

The high performance level of the C6711 made it easy to write code for this application. It was not necessary to be significantly concerned about meeting the performance requirement (completing all data acquisition and calculations for each feedback loop in less than 2.6 ms). The code was written entirely in the C programming language (no assembly language was required). The C compiler for the C6711 is convenient to use: it includes dozens of libraries for math and chip support, fully integrated debugging capabilities and provides several levels of optimization depending on the needs of the user.

2.2. Voltage-controlled oscillator (VCO)

A schematic of the VCO board is shown in figure 3. The two control inputs from the D/A converter (PL2, FAdj and PL3, IIn) must be buffered and level-shifted, since the converter operates from a single supply and cannot output a bipolar voltage or even a voltage near zero. These inputs must be converted from the unipolar codec output (0.64–4.2 V) to (a) a $\pm 2 \text{ V}$ bipolar voltage for application to the sweep input (FAdj) of the VCO and (b) a calibrated current for input to the centre frequency control (IIn) of the VCO.

The VCO is a Maxim MAX038 high-frequency sinusoidal waveform generator (U1) with a centre frequency sweep range of more than 350–1, with the actual centre frequency range set by a single high-quality capacitor. The output of the VCO, which is nominally 1 V peak, is sent to an Analog Devices AD845 operational amplifier (U2), which is configured to allow amplitude adjustment (via variable resistor VR4) from 0 to 10 V peak at the output connector (PL4). Regulators U8 and U9 and Zener diodes ZD1 and ZD2 generate the $\pm 5 \text{ V}$ needed by the VCO from the external $\pm 15 \text{ V}$ power applied to the VCO board. All other circuitry on the VCO board is powered from the external $\pm 15 \text{ V}$ supply.

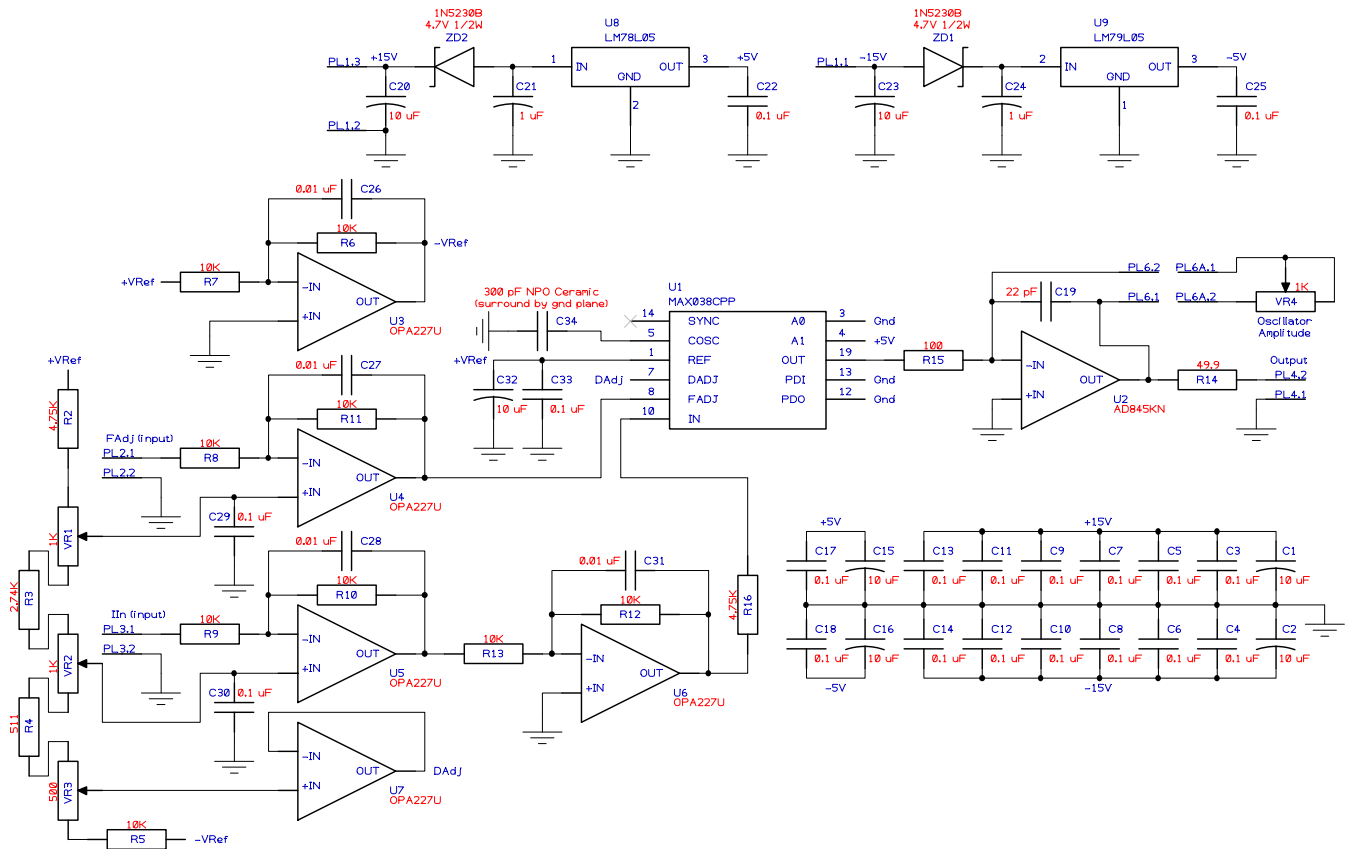


Figure 3. Schematic of the voltage-controlled oscillator board.

The VCO is controlled by three inputs: (1) the FAdj input on pin 8 of U1, used for agile frequency adjustment, (2) the IIn input on pin 10, used for wide range frequency control and (3) the DAdj input on pin 7, used for duty cycle adjustment. The frequency range is chosen by C34, which is a high quality, ceramic NPO (‘negative positive zero’, referring to the near-zero temperature coefficient of capacitance) capacitor.

In order to offset the input voltages properly, a series of adjustable voltages are derived from a bipolar reference voltage applied across a string of variable resistors. The 2.50 V reference voltage is conveniently supplied by a band gap voltage reference within the MAX038 on pin 1. This voltage is inverted by amplifier U3 to provide ± 2.50 V (designated $\pm V_{Ref}$ in figure 3). This stable, bipolar reference voltage is applied across the resistor string made up of R2, R3, R4 and R5 precision 1% metal-film resistors, and VR1, VR2 and VR3 20-turn precision trim pots. The FAdj pin requires ± 2 V to adjust the frequency deviation about the centre frequency by about $\pm 60\%$. We reduce this voltage by a small amount (to approximately ± 1.7 V), in order to provide a maximum frequency deviation of $\pm 50\%$, which is adjustable down to zero in the software. A TI/Burr-Brown OPA227 low-noise, precision operational amplifier (U4) is configured as a unity-gain inverting buffer. Its non-inverting input connects to the centre tap of variable resistor VR1, nominally adjusted to about 1.2 V. This arrangement effectively shifts the 0.64–4.2 V input to about ± 1.7 V.

The IIn input pin programs the centre frequency of oscillation. This input acts as a virtual short, internally

maintaining a voltage burden of less than ± 2 mV to ground. It is driven by amplifiers U5 and U6 and resistor R16. U5, with its non-inverting input tied to variable resistor VR2 (nominally adjusted to 0.3 V), converts the 0.64–4.2 V input on PL3 to approximately 0 to -3.6 V. This voltage is inverted by U6, sourcing a positive current from zero to more than $750 \mu\text{A}$ into the IIn input via R16. The frequency is computed from the relationship $f = I_{In}/C34$. With the nominal value for C34 of 250 pF, the frequency extends from below 3 kHz to over 3 MHz.

The DAdj pin requires an adjustable voltage near zero to set the duty cycle of the sinusoidal waveform. This adjustment can be used to minimize the harmonic distortion in the output. Variable resistor VR3, which can be adjusted by approximately ± 60 mV, is set to provide exact 50% symmetry, minimizing the second harmonic. Operational amplifier U7 is necessary to drive the DAdj input, which draws about $250 \mu\text{A}$ of current; a variable resistor alone cannot provide a temperature-stable adjustment. The DAdj adjustment has a small effect on the output frequency, so VR3 is adjusted prior to the adjustment of VR1 and VR2.

We discovered early into the VCO design phase that the centre frequency versus tuning voltage characteristic of the VCO becomes unacceptably nonlinear at very low (< 25 kHz) and very high (> 2.5 MHz) frequencies. This discovery necessitated two changes to the overall design. The first involved the centre-frequency tuning voltage sent to the AFM image port. This voltage was found to be nonlinear with frequency and was thus not accurate enough for our needs,

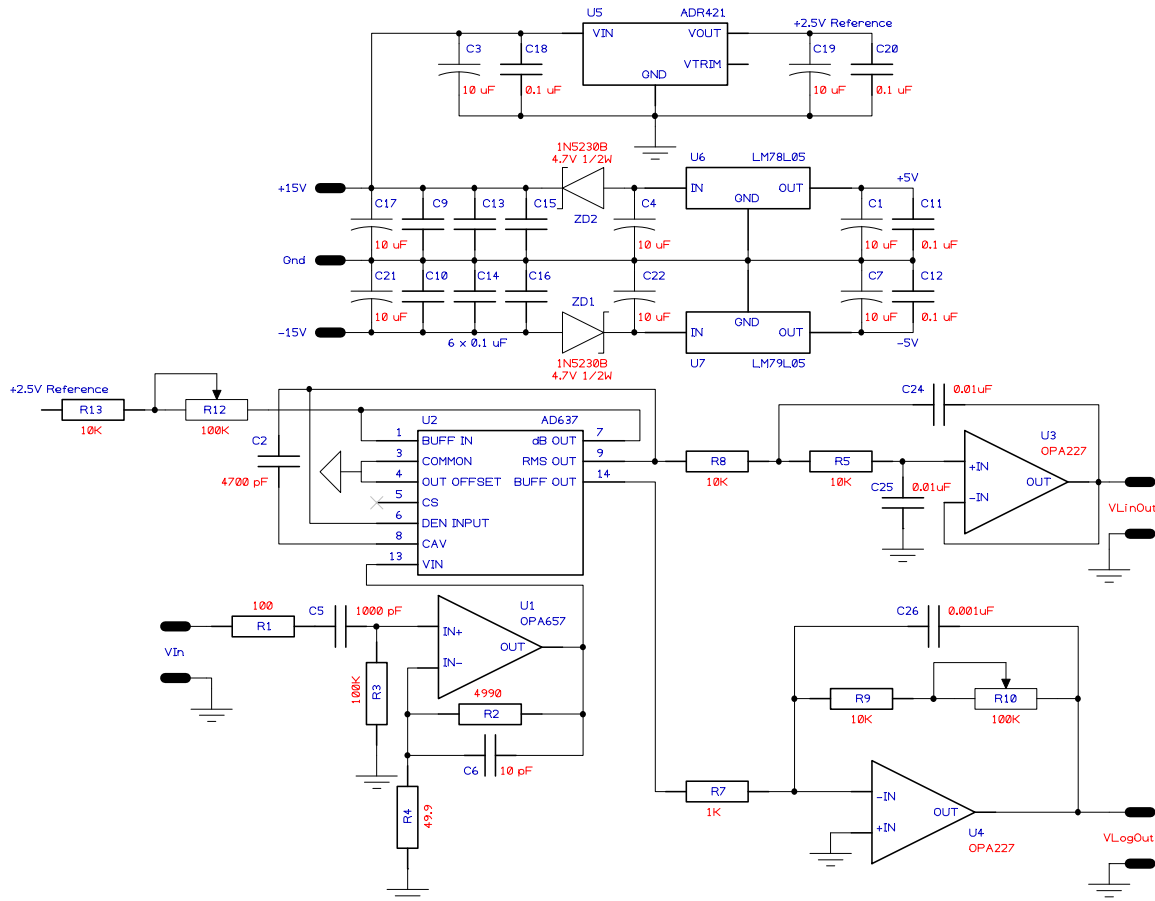


Figure 4. Schematic of the rms-to-dc converter board.

given our quantitative emphasis. Therefore, the output was changed to a 16-bit codec on the DSK motherboard that had been previously unused. This 8 kHz, voice quality codec was too slow to use in place of the PCM3003 and included only one channel of the D/A converter output. However, it could provide a very linear output to the AFM image port and could be calibrated in the software for gain and offset. Its output was calibrated to provide a voltage equal to the frequency in megahertz, i.e., 1 V = 1 MHz. Second, since the VCO centre frequency versus tuning voltage characteristic was unacceptably nonlinear, a 65-point, linear interpolation look-up table was used to calibrate the VCO tuning voltage in the software. The voltage necessary to give the proper frequency, as measured on a six-digit frequency counter, was measured at 65 appropriately chosen points and stored in an array in DSP memory along with an array containing the corresponding frequencies. These arrays are indexed in order, allowing the DSP to quickly find the two appropriate frequency-voltage points and linearly interpolate between them. The 65-point look-up table provides accuracy to better than 0.1% of the centre frequency.

2.3. RMS-to-dc converter

Figure 4 shows a schematic diagram of the rms-to-dc converter circuit. The high-source-impedance output from the AFM photodiode detector is capacitively coupled into a high-bandwidth, low-noise, FET-input operational amplifier U1

(TI/Burr-Brown OPA657) with a non-inverting gain of 101. The ac-coupled input is centred at ground via R3, which also sets the input impedance of this amplifier to about 100 kΩ. Regulators U6 and U7 and Zener diodes ZD1 and ZD2 provide the ±5 V required by the OPA657 from the external ±15 V power supplied to the board.

The AFM photodiode signals seen in our measurements are typically less than 100 mV in amplitude and sometimes as small as a few millivolts. Therefore, a relatively expensive, high-gain, low-noise, front-end amplifier (U1) is required to amplify the signal before processing by the DSP-RTS. The output of the amplifier U1 is applied to a high-precision, wideband rms-to-dc converter U2 (Analog Devices AD637). This rms-to-dc converter has the property that its error/bandwidth response depends on input level (e.g., ±3 dB at 1 MHz for 0.2 Vrms and ±3 dB at 8 MHz for 2 Vrms). The need for a flat frequency response to 3 MHz is one of the primary reasons for the high gain of the input amplifier.

The settling time/averaging time for the AD637 rms-to-dc converter is determined by R5, R8, C2, C24 and C25. These components were chosen to allow three to five time constants for settling during each resonant trace scan at the 375 Hz (2.7 ms) trace scan rate. U3 constitutes a unity-gain, low-noise Sallen–Key filter, which provides the linear output for this board. The AD637 also includes a logarithmic (dB) output that requires a calibrated reference voltage in order to convert the linear input voltage into a dB output. An Analog

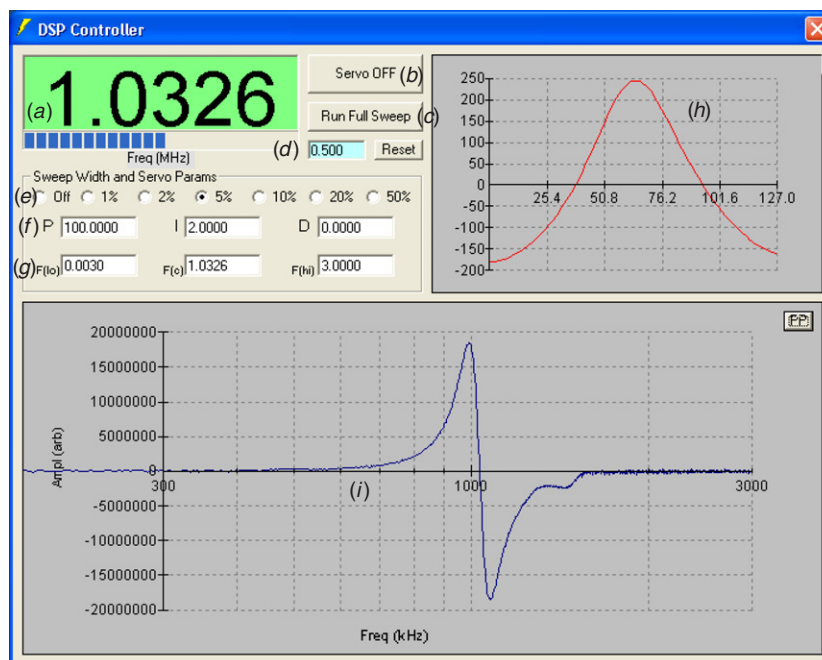


Figure 5. Screen shot of the host control program. Controls for activating the servo (*b*), setting PID parameters (*f*) by means of a figure of merit (*d*), adjusting frequency limits (*g*) and sweep width (*e*), and performing (*c*) and viewing (*i*) a full sweep are visible, along with frequency (*a*) and resonance curve readouts (*h*).

Devices ADR421 ultraprecision, low-noise, low-drift 2.5 V voltage reference (U5) is used and is calibrated to give -2 V at 1 mV input, -1 V at 10 mV input, 0 V at 100 mV and $+1$ V at 1 V input (all input levels are rms). Inverting-amplifier U4 and R10 provide the dB gain adjustment and U5 and R12 provide the dB reference adjustment.

The completed rms-to-dc converter was measured and yielded a linear voltage response from about 1 mV to 3 V with a flat frequency response over a frequency range of approximately 1 kHz to 3.2 MHz (3 dB). Both linear and logarithmic outputs are applied to the PCM3003 daughter-card stereo L-R inputs.

3. Experimental procedure and software

The DSP-RTS is designed to work with an existing AFM with no modifications to the AFM. As mentioned above, the input signal to the DSP-RTS is the unfiltered photodiode signal. As shown in figure 1, the frequency-proportional output of the DSP-RTS is connected to the auxiliary image port of the AFM and is used to acquire the contact-resonance-frequency image. The host control software for the DSP-RTS is activated after the AFM tip is brought into contact with the sample with an appropriate amount of applied force on the tip.

A computer screen image for the host control program is shown in figure 5. Not shown in the figure is the manual adjustment for the VCO output voltage, which is a potentiometer (VR4 in figure 3) mounted on the DSP-RTS enclosure. This control is initially adjusted to provide a weak oscillator amplitude in order to prevent the AFM tip from being vibrated out of contact with the sample. To characterize the contact-resonance spectrum, the <Run Full Sweep> button (*c*) is activated and a frequency sweep is performed over the

full 3 kHz to 3 MHz range (*i*). It is important to choose an appropriate sweep width percentage (*e*) during this procedure. If the width is too large, there will be a stronger signal, but the frequency resolution will be poor. An appropriate choice is usually 1 or 2%. Often the frequencies of the resonant peaks are already known. In this case, the full sweep function can be performed as a crosscheck.

After performing a full frequency sweep, the user chooses a resonant frequency to track and sets a limiting window around this peak. This limiting window prevents the DSP-RTS from accidentally tracking an adjacent, but undesired, peak. The limiting window can be selected graphically or by entering the centre, low and high frequencies, in the F(*c*), F(*lo*) and F(*hi*) text blocks, respectively (*g*). After the limiting window is selected, the PID parameters are adjusted and the <Servo On/Off> button (*b*) is activated.

It is essential to set the PID parameters (*f*) for the tracking feedback appropriately. For example, if the proportional (P) parameter is set too large, the system may become unstable or even oscillate. To assist in the choice of these parameters, a figure-of-merit (*d*) is available, which is derived from the rms deviation of the tracked peak from the centre. With 128 data points numbered 0–127, a perfectly centred peak would occur at 63.5. Since this centre is not an integer, the feedback loop will never reach zero error and will always provide a correction. Typically, the I and D parameters are set to zero and the proportional (P) parameter is increased until the onset of oscillation. It is then reduced by about half, and then the I and D parameters are increased. Parameter adjustment is done iteratively, until the PID settings are appropriate for the sample and imaging speeds being used.

The sweep width percentage adjustment (*e*) can be set between 1% and 50% in a 1-2-5 sequence. It is used to set the

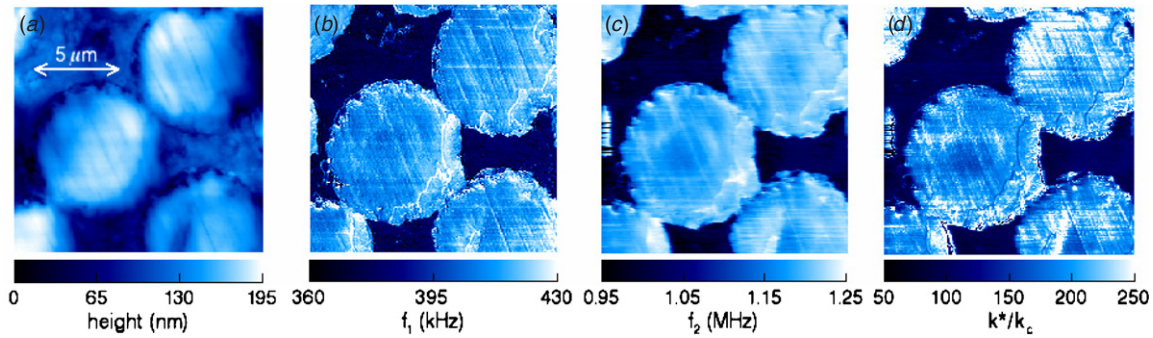


Figure 6. Images of glass fibre/polymer matrix composite. (a) AFM topography. (b) Contact-resonance-frequency image for the first (lowest) flexural mode f_1 . (c) Contact-resonance frequencies for the second flexural mode f_2 . (d) Normalized vertical contact stiffness k^*/k_c calculated from (b) and (c); from [7].

frequency deviation about the centre frequency. For example, if the centre frequency is set to 1 MHz and the sweep width is set to 10%, then the frequency sweeps between 0.9 and 1.1 MHz ($1 \text{ MHz} \pm 100 \text{ kHz}$). Given that 128 points are acquired in each sweep, the frequency resolution is about 1.6 kHz in this example.

The host control software that communicates with the DSK is written in Microsoft Visual BASIC. A Windows 32-bit application programming interface in the form of a dynamic link library is provided by TI to communicate with the DSK using popular languages such as C and Visual BASIC. Several functions are provided, including resetting the DSP/DSK, loading an executable program into the DSK and read/write access of the memory on the DSK.

We used TI's Code Composer Studio development environment to design the real-time control software that runs on the DSK. Two-way communication between the real-time and host software is facilitated via a shared memory space and a simple semaphore mechanism. The main consideration in this design was to guarantee that the real-time software never waits or depends on the host software for proper operation. In fact, the Visual BASIC host software and the entire Windows operating system can be shut down, rebooted and re-connected to the real-time DSP-RTS without a single resonance-tracking cycle being affected.

A calibration device is also included with the DSP-RTS. This device, which incorporates a sealed, two-port resonant circuit (consisting of passive components) with three switch-selectable resonant frequencies, was carefully characterized using a network analyser with a precise, synthesized sweep frequency generator. The device can be substituted in place of the AFM photodiode signal and is used to verify that the DSP-RTS is working properly. It can also be used to measure the step-response associated with the PID parameters. Because the calibration device avoids wear and tear of the AFM tip, it is an ideal tool to acquire familiarity with the DSP-RTS prior to experimentation.

4. Example images

A glass-fibre/polymer matrix composite sample [7] was used to test the system. The sample was formed by embedding glass fibres in a polymer matrix. Cylindrical specimens of

fibre composites were prepared by pouring a polymer mixture into plastic cylinders. Prior to the introduction of the polymer mixture, the glass fibres were aligned in the centre of the plastic cylinder and secured at both ends. The samples were then left to cure at room temperature for about three days. Samples 2 cm in height were then cut from the cylindrical sample and polished manually.

Figure 6(a) contains an image of the topography of one region of the composite sample. The image was acquired with the AFM tip in contact with the sample (contact mode). It can be seen that the chemical-mechanical polishing process resulted in a surface in which the glass fibres were consistently 150–200 nm higher than the epoxy matrix. All of the images in figure 6 were acquired with a rectangular AFM cantilever micromachined from single-crystal silicon. The cantilever was approximately $225 \mu\text{m}$ long, $28 \mu\text{m}$ wide and $3 \mu\text{m}$ thick. A nominal value for the cantilever spring constant $k_c = 2.8 \text{ N m}^{-1}$ was supplied by the vendor. The values for the lowest two free-space (out of contact) resonant frequencies for this cantilever were $85.64 \pm 0.01 \text{ kHz}$ and $531.46 \pm 0.01 \text{ kHz}$, respectively.

Two contact-resonance-frequency images acquired with the DSP-RTS for the glass-fibre/polymer matrix composite sample are shown in figures 6(b) and (c). The image in figure 6(b) was acquired while tracking the lowest flexural contact resonance f_1 . In both figures 6(b) and (c), brighter colours indicate higher contact-resonance frequencies. As indicated in the scale in figure 6(b), f_1 ranged from approximately 360 kHz to 430 kHz. The image in figure 6(c) represents the values of the second flexural mode f_2 . In this case, f_2 ranged from 0.95 MHz to 1.25 MHz. The image of f_1 appears somewhat 'sharper' than that of f_2 ; this is due to the specific choice of PID parameters for each image.

The experimental contact-resonance frequencies are interpreted with an analytical model for the cantilever beam dynamics [1, 2]. The beam-dynamics model relates the measured frequencies to one or more parameters that characterize the tip-sample interaction. The simplest model to describe the interaction is a spring of stiffness k^* between the tip and the sample, representing a purely elastic interaction. This analysis yields values of k^*/k_c , the contact stiffness normalized by the cantilever spring constant. From the values of k^*/k_c , elastic properties of the sample can be calculated with

the help of a model to describe the contact mechanics between the tip and sample. Hertzian (spherical) contact mechanics are usually invoked. Although, in principle, k^* could be determined from a single contact-resonance frequency, in practice information from two contact resonances are needed to obtain k^* . This practice compensates for the fact that the AFM tip is not located at the exact end of the cantilever [1, 2].

From the contact-resonance-frequency images, an image of the normalized contact stiffness k^*/k_c can be calculated by applying the analysis model on a pixel-by-pixel basis. Figure 6(d) shows the contact stiffness image calculated from figures 6(b) and (c) in this way. The image indicates that the glass fibres are stiffer than the polymer matrix. It also reveals slightly more compliant (softer) regions inside the fibres. Note that evidence of the more compliant regions is absent from the topographic image in figure 6(a). This simple example illustrates the ability of our techniques to provide useful mechanical-property information.

5. Discussion

Our DSP-based methods have several distinct advantages over other approaches [1, 3, 5, 6]. The most important is the speed of image acquisition. If we allow 4–7 servo time constants (2.66 ms) per image pixel, the DSP-RTS can acquire a 256×256 pixel image in 20–25 min. The optimum scan speed depends on experimental parameters such as scan length, surface roughness and sample properties. However, we have found that this rate (approximately 0.2 Hz) is usually suitable for micrometer-sized scans. Reducing the number of points in the resonance curve from 128 to 64 and implementing curve fitting for frequency interpolation would reduce the acquisition time to about 10 min.

In addition, DSP-based methods provide greater flexibility than analogue approaches. Adding additional capability is often as simple as changing the software. For example, the upgrade to Lorentzian or other curve fitting (making use of all 128 data points) instead of tracking the peak only (using only one data point) can be facilitated with a software upgrade. This upgrade alone could have a major impact on the signal-to-noise ratio seen in the acquired images. As another example of a software upgrade, our methods could also be easily extended to directly calculate the resonant Q -factor of the cantilever [3]. Q -factor values provide information about the damping coefficient between the tip and the sample. Such information can provide insight into the tip–sample adhesive forces as well as the viscoelastic properties of the sample. This upgrade could be included by simply adding another analogue output (D/A converter) channel and placing a voltage proportional to the calculated Q -factor on this output.

The contact-resonance frequency depends on several factors, including the type of cantilever used, the choice of resonant mode (number and type—flexural, torsional or lateral), the sample elastic modulus and the contact conditions. It is imperative that the system be able to quickly and reliably track the resonance and accurately measure the centre frequency. The DSP-RTS can track very large (hundreds

of kilohertz), instantaneous shifts in the contact-resonance frequency without error. In contrast, heterodyne techniques [3, 5] offer exceptional frequency resolution at the expense of dynamic range and speed.

Exceptional frequency resolution and outstanding dynamic range can be achieved simultaneously, however. An upgrade to our system, currently underway, involves replacing the current analogue VCO with an oscillator based upon direct digital synthesis techniques [9] for frequency generation. This upgrade will improve the intrinsic frequency resolution from our current value of about 12 Hz to about 2 mHz, completely remove all nonlinearities associated with frequency generation, improve frequency accuracy by more than five orders of magnitude and significantly reduce harmonic distortion.

In summary, the DSP-RTS is a fast, accurate, versatile, *quantitative* method for imaging of mechanical properties with nanoscale spatial resolution. Further improvements to this system will add value to both the DSP-RTS and the general application of AFM to mechanical-property imaging.

Acknowledgments

The glass-fibres/polymer composite sample was provided by J A Turner (University of Nebraska-Lincoln) and prepared by C N McCowan (NIST). This work is a contribution of NIST, an agency of the US government, and is not subject to copyright.

References

- [1] Rabe U, Kopycinska M, Hirsekorn S, Muñoz Saldaña J, Schneider G A and Arnold W 2002 High-resolution characterization of piezoelectric ceramics by ultrasonic scanning force microscopy techniques *J. Phys. D: Appl. Phys.* **35** 2621
- [2] Hurley D C, Shen K, Jennett N M and Turner J A 2003 Atomic force acoustic microscopy methods to determine thin-film elastic properties *J. Appl. Phys.* **94** 2347
- [3] Yamanaka K, Maruyama Y, Tsuji T and Nakamoto K 2001 Resonance frequency and Q factor mapping by ultrasonic atomic force acoustic microscopy *Appl. Phys. Lett.* **78** 1939
- [4] Hurley D C, Kopycinska-Müller M, Kos A B and Geiss R H 2005 Nanoscale elastic-property measurements and mapping using atomic force acoustic microscopy methods *Meas. Sci. Technol.* **16** 2167
- [5] Kobayashi K, Yamada H and Matsushige K 2002 Resonance tracking ultrasonic atomic force microscopy *Surf. Interface Anal.* **33** 89
- [6] Passeri D, Bettucci A, Germano M, Rossi M, Alippi A, Sessa V, Fiori A, Tamburri E and Terranova M L 2006 Local indentation modulus characterization of diamondlike carbon films by atomic force acoustic microscopy two contact resonance frequencies imaging technique *Appl. Phys. Lett.* **88** 121910
- [7] Hurley D C, Kopycinska-Müller M, Kos A B and Geiss R H 2005 Quantitative elastic-property measurements at the nanoscale with atomic force acoustic microscopy *Adv. Eng. Mater.* **7** 713
- [8] Hurley D C, Kopycinska-Müller M, Langlois E D, Kos A B and Barbosa N 2006 Mapping substrate/film adhesion with contact-resonance-frequency atomic force microscopy *Appl. Phys. Lett.* **89** 021911
- [9] Tierney J, Rader C M and Gold B 1971 Digital frequency synthesizer *IEEE Trans. Audio Electroacoust.* **19** 48